Chemical Engineering Science 327 (2026) 123637

Contents lists available at ScienceDirect

Chemical Engineering Science

journal homepage: www.elsevier.com/locate/ces

Performance assessment and modelling of CO_2 capture via temperature swing adsorption using biowaste-based materials

Ana S. Amorim [a], Rui M. Filipe [b,*], Cintia K. Rojas-Mayorga [c], Didilia I. Mendoza-Castillo [d], Adrián Bonilla–Petriciolet [d], Henrique A. Matos [e]

[a] c5Lab – Sustainable Construction Materials Association, 2795-242 Linda-a-Velha, Portugal
[b] CERENA, Instituto Superior de Engenharia de Lisboa, Instituto Politécnico de Lisboa, 1959-007 Lisbon, Portugal
[c] Universidad de Colima, Facultad de Ciencias Químicas, C.P. 28400 Coquimatlán, Colima, Mexico
[d] Tecnológico Nacional de México - Instituto Tecnológico de Aguascalientes, Departamento de Ingeniería Química, C.P. 20256 Aguascalientes, Mexico
[e] CERENA, Instituto Superior Técnico, Universidade de Lisboa, 1049-001 Lisbon, Portugal

ARTICLE INFO

Keywords:
Biowaste-based adsorbents
CO_2 capture
Cement plant
Lanthanum functionalization
Multicyclic adsorption
Kinetic-based modelling

ABSTRACT

The multicyclic kinetic performance and equilibrium CO_2 adsorption capacities of different biowaste-based adsorbents were measured experimentally, modelled and compared using pure CO_2 streaming and cement plant flue gas. Biowaste-based adsorbents used for CO_2 capture were synthesized from cork stoppers, grape marc, and rice husks via pyrolysis and hydrothermal carbonization with and without lanthanum functionalization. The results demonstrate that pyrolysis is a more effective method than hydrothermal carbonization for producing CO_2-capturing adsorbents from tested biowastes. These adsorbents can reach equilibrium CO_2 carrying capacities of up to 63 mg/g at atmospheric temperature and pressure. No deactivation was observed over five adsorption/desorption cycles for cork- and rice husk-based adsorbents and the deactivation observed for grape marc-based adsorbents under flue gas can be overcome via lanthanum functionalization. Kinetic parameters for CO_2 adsorption on biowaste-based adsorbents were calculated and compared to identify the impact of micropores and mesopores on separation performance.

1. Introduction

Climate change is a major global challenge that must be addressed urgently, and controlling greenhouse gas emissions is essential to achieving the sustainable goals defined by the Paris Agreement. Under this agreement, European Union countries must become carbon–neutral by 2050 (Zuazua Ruiz et al., 2023). Approximately, 38 Gton of CO_2 were emitted into the atmosphere worldwide in 2023, and these emissions are still rising (CO2 emissions - Our World in Data, 2023). The cement industry's contribution to the CO_2 global emissions has been increasing in the past years and it reached 7–8 % of the total emissions, making it the second major industrial source of CO_2 emissions, after the iron and steel sector (Annual CO2 emissions from cement, 2023).

Carbon capture, utilization, and sequestration are among the main strategies used to control CO_2 emissions and mitigate their environmental impact (Krishnan et al., 2023; Dhingra and Kumar, 2025). Adsorption is a cost-effective carbon-capture technology due to its simplicity, performance, stability, safety, low environmental impact, and reduced costs (Sifat and Haseli, 2019). In this process, CO_2 molecules in the flue gas are captured by forming a thin film on the surface of a porous material. The driving force for adsorption is the intermolecular forces between the particles, and it is dependent on the temperature, pressure, and characteristics of the adsorbent (e.g., pore size, surface chemistry) (Liu et al., 2025; Li et al., 2021). For continuous operation, two columns are required, one for adsorption and the other for desorption. The shift between adsorption and desorption is performed by changing either the temperature or pressure, for example, via temperature swing adsorption (TSA) (Zhang and Wang, 2025); pressure swing adsorption (PSA) (Si et al., 2025); or vacuum swing adsorption (VSA) (Ren et al., 2025). In TSA, the desorption column is heated with sweep gas to desorb the CO_2 molecules (Zhao et al., 2019). On the other

Abbreviations: FTIR, Fourier-Transform Infrared Spectroscopy; HTC, Hydrothermal Carbonization; MOF, Metal-Organic Framework; MSE, Mean Squared Error; PSA, Pressure Swing Adsorption; SEM, Scanning Electron Microscopy; TGA, Thermogravimetric Analysis; TSA, Temperature Swing Adsorption; VSA, Vacuum Swing Adsorption; XRD, X-Ray Diffraction.

* Corresponding author.
E-mail address: rfilipe@isel.ipl.pt (R.M. Filipe).

https://doi.org/10.1016/j.ces.2026.123637
Received 16 July 2025; Received in revised form 30 January 2026; Accepted 16 February 2026
Available online 20 February 2026

Nomenclature

C_o	Gas concentration of the thermogravimetric analyzer, mol/m^3
C_{FG}	CO_2 concentration of the flue gas, mol/m^3
$C_{f,t}$	CO_2 concentration at the exit of the thermogravimetric analyzer at time t, mol/m^3
C_t	CO_2 concentration at time t, mol/m^3
$F_{CO_2,i}$	CO_2 flowrate at the entry of the thermogravimetric analyzer, mol/s
F_{inert}	Inert gas flowrate, mol/s
k_1	Pseudo first order adsorption kinetic constant, s^{-1}
k_{1,CO_2}	Pseudo first order adsorption kinetic constant using a pure CO_2 stream, s^{-1}
$k_{1,FG}$	Pseudo first order adsorption kinetic constant using a flue gas stream, s^{-1}
$k_{1,m}$	Pseudo first order adsorption kinetic constant in the mesopores, s^{-1}
$k_{1,\mu}$	Pseudo first order adsorption kinetic constant in the micropores, s^{-1}
k_2	Pseudo second order adsorption kinetic constant, s^{-1}
k_a	Adsorption kinetic constant, m^3·mol^{-1}·s^{-1}
k_d	Desorption kinetic constant, s^{-1}
M_{w,CO_2}	Molecular weight of CO_2, mg/mol
m_{char}	Mass of adsorbent obtained after pyrolysis or hydrothermal carbonization, g
m_i	Mass of adsorbent used for the thermogravimetric analysis, mg
m_{min}	Minimum mass of adsorbent determined in the thermogravimetric analyzer, μg
$m_{precursor}$	Mass of biowaste fed to pyrolysis or hydrothermal carbonization, g
n	Order of reaction, –
q_e	Equilibrium adsorbent carrying capacity, mg CO_2/g adsorbent
q_{e,CO_2}	Equilibrium adsorbent carrying capacity using a pure CO_2 stream, mg CO_2/g adsorbent
$q_{e,FG}$	Equilibrium adsorbent carrying capacity using a flue gas stream, mg CO_2/g adsorbent
$q_{e,m}$	Equilibrium adsorbent carrying capacity in the mesopores, mg CO_2/g adsorbent
$q_{e,\mu}$	Equilibrium adsorbent carrying capacity in the micropores, mg CO_2/g adsorbent
q_{max}	Maximum adsorbent carrying capacity, mg CO_2/g adsorbent
q_t	Adsorbent carrying capacity at time t, mg CO_2/g adsorbent
r_a	Rate of adsorption, s^{-1}
$r_{CO_2,cap,t}$	Rate of CO_2 capture in the thermogravimetric analyzer at time t, mol/s
r_d	Rate of desorption, s^{-1}
T	Temperature, K
t	Time, s
$x_{CO_2,f,t}$	CO_2 molar composition of the gas stream leaving the thermogravimetric analyzer, –
$x_{CO_2,i}$	CO_2 molar composition of the gas stream entering the thermogravimetric analyzer, –
Y	Yield, %

Greek letters

Δm_t	Variation of adsorbent mass in the thermogravimetric analysis at time t, μg
θ_t	Occupied sites in the adsorbent surface at time t, –

hand, the pressure change is performed by either increasing the pressure in the adsorption column (PSA) or by operating under vacuum in the desorption column (VSA) (Ketabchi et al., 2023).

Popular adsorbents for PSA, VSA and TSA include carbonaceous materials, zeolites, and metal–organic frameworks (MOFs) (Si et al., 2025; Henrotin et al., 2024; Paz et al., 2024). Recent studies have focused on carbon biomass-based adsorbents, because biomass is an abundant, renewable, and inexpensive resource (Li et al., 2021; Akdag et al., 2022; Zhu et al., 2023; Li et al., 2025). These adsorbents are reported to display CO_2 adsorption capacities up to 0.48 g/g at atmospheric pressure (Quan et al., 2023). They can be obtained via pyrolysis (biochar) or hydrothermal carbonization (hydrochar) (Li et al., 2021; Quan et al., 2023). Biomass-based adsorbents offer advantages for the operation of CO_2 capture units. For example, the multicyclic performance of hazelnut shell-based activated carbon was evaluated in the literature using both PSA and TSA, and no adsorbent deactivation was found over consecutive cycles (Akdag et al., 2022). On the other hand, Querejeta et al. (Querejeta et al., 2024) studied the experimental CO_2 capture capacity of adsorbents derived from pine cone leaves and pine kernel shells using pure and diluted CO_2 streams (10 and 30 % CO_2), which intended to simulate post-combustion conditions. The results show a CO_2 capture capacity decrease of 34–37 % when using a 30 % CO_2 stream and a reduction of 61–64 % when using a 10 % CO_2 stream, when compared to a pure CO_2 stream. Nevertheless, it is convenient to remark that the flue gas from an industrial plant contains other impurities and, consequently, the adsorbent performance should be tested under real operating conditions. To the best of the authors' knowledge, no study was conducted to evaluate the adsorption capacity of biomass-based adsorbents directly from industrial cement plant flue gas. Also, the activity over multiple adsorption/desorption cycles should be analyzed for biomass-based adsorbents that have been prepared using different precursors and synthesis routes with the aim of identifying the best option.

Previous studies have proved that CO_2 adsorption properties can be improved if proper surface functionalization is performed (Li et al., 2021; Zhu et al., 2023; Li et al., 2025). For instance, lanthanum doping has led to a positive effect on MOFs' stability and surface properties for CO_2 capture (Wang et al., 2019). The functionalization of biomass-based adsorbents with lanthanum has been also applied for removing other relevant environmental pollutants, such as fluoride and arsenic (Mendoza-Castillo and Reynel-Ávila, 2019; Merodio-Morales et al., 2022). However, no study was found in the literature concerning the effect of lanthanum functionalization in CO_2 adsorption properties of biowaste-based adsorbents.

This work aims to address the literature gaps by modelling the multicyclic CO_2 capture kinetics of biowaste–based adsorbents from pure CO_2 and a real cement plant flue gas. Residues of rice husk, cork stoppers, and grape marc were utilized for the adsorbent preparation via pyrolysis and hydrothermal carbonization, with and without lanthanum functionalization. CO_2 adsorption properties of biowaste-based adsorbents were measured experimentally, simulated using a kinetic-based model and compared.

2. Materials and methods

2.1. Preparation and characterization of adsorbents

A full-factorial design of experiments was applied to study the influence of the precursor, the char production method, and the lanthanum functionalization on CO_2 capture efficiency of biowaste-based adsorbents (Fig. 1). Three different biomass residues were studied as adsorbent precursors: rice husk, cork stoppers, and grape marc.

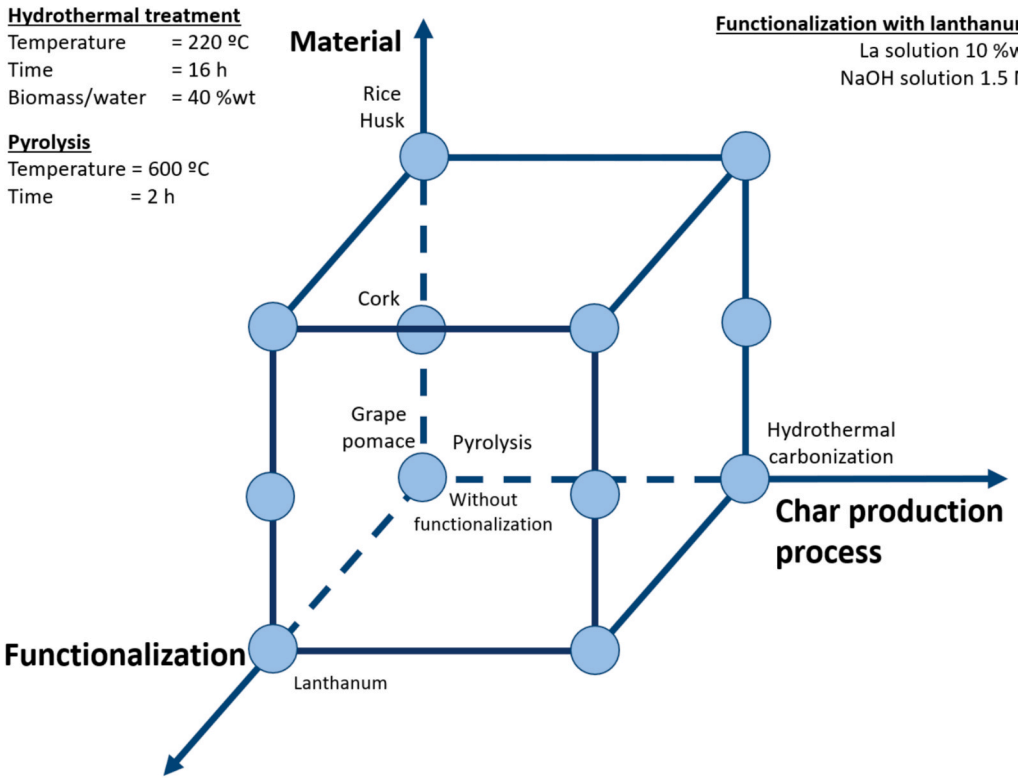

Fig. 1. Design of experiments used to produce biowaste-based adsorbents for CO_2 capture.

The char production process included pyrolysis or hydrothermal carbonization (HTC). For both routes, the precursors were submitted to cleaning with water, dried and particle size reduction. The pyrolysis was performed at 600 °C for 2 h, with a heating rate of 10 °C/min in a Carbolite Eurotherm tubular furnace under N_2 atmosphere. The pyrolysis temperature was chosen based on literature studies which indicated that 600 °C ensures the biowaste materials are already pyrolyzed (Madadian et al., 2022; Mansaray and Ghaly, 1998; Shangguan et al., 2018). On the other hand, HTC was conducted in a 500 mL Hydrion Scientific reactor at 220 °C for 16 h with a biowaste–to–water ratio of 40 % (by mass) (Diaz et al., 2019). These HTC conditions were chosen to favor the development of adsorbent textural parameters, which can be positively correlated with CO_2 capture (Drage et al., 2009). The HTC residence time was selected to ensure that the hydrothermal carbonization of the material was complete regardless of the feedstock, since long residence times can result in the development of better structural properties (Gao et al., 2013). The pyrolysis and HTC yields were calculated using Equation (1)

$$Y = \frac{m_{char}}{m_{precursor}} \times 100 \quad (1)$$

where m_{char} corresponds to adsorbent mass (g) obtained after pyrolysis or HTC and $m_{precursor}$ is the precursor mass (g) used in the corresponding carbonization process. Lanthanum functionalization was applied to modify adsorbent surface properties for CO_2 adsorption. The methodology of this procedure was described by Merodio-Morales et al. (Merodio-Morales et al., 2022). Firstly, a 10 % (by mass) lanthanum aqueous solution was prepared using La(NO3)3··6H2O and then 10 g of biowaste-based char was added to the solution. After 30 min of agitation to promote homogenization, a 1.5 M NaOH solution was added dropwise until precipitation occurred. After 1 h of agitation, the samples were filtered to separate the adsorbents.

All the adsorbent samples, with and without La-functionalization, were washed with deionized water, dried at 100 °C, and sieved to obtain a particle size of 420–500 μm. The sieving of the samples was performed to standardize them, allowing the comparison across the different experiments. The selected particle range is in line with the particle size considered by Manyà et al. (Manyà et al., 2020). Selected samples of biowaste-based adsorbents were analyzed by X-ray Diffraction (XRD) to identify the crystalline structures. XRD analysis was performed using a Bruker D8-Advance with mirror Göebel, equipped with a cooper anode RX and CuKα radiation (λ = 1.5406 Å). The diffractograms were obtained on a °2θ range between 10 and 80. On the other hand, Fourier Transform Infrared (FTIR) was applied to identify the functional groups (i.e., surface chemistry) of adsorbents surfaces. All FTIR spectra were recorded with spectroscopic grade KBr using a Bruker IFS 66/S spectrophotometer obtaining 200 scans with 4 cm^{-1} resolution. The specific surface area of the biowaste-derived adsorbent samples was determined by N_2 physisorption measurements conducted at –196 °C in a Micrometrics ASAP 2020 porosimeter. The morphology of selected adsorbent samples was also analyzed by scanning electron microscopy.

2.2. Experimental CO_2 carrying capacity

CO_2 carrying capacity of biowaste-based adsorbents and their performance in TSA over consecutive adsorption/desorption cycles were evaluated using a thermogravimetric analyzer (TGA). Each adsorption/desorption cycle begins with heating the sample to the desorption temperature. Once the temperature is reached, desorption is carried out under a N_2 atmosphere. The system is then cooled back to the atmospheric temperature and then adsorption is conducted under a CO_2 atmosphere. The operating conditions of adsorption and desorption cycles for the adsorbents prepared without and with lanthanum functionalization are presented in Table 1 and Table 2, respectively. Flowrates of 200 mL/min were used in the experiments to provide the specified atmosphere for each cycle step.

TGA gave information about the mass variation due to the adsorption and desorption of CO_2. The carrying capacity of each adsorbent, q_t (mg/g), was calculated over time via Equation (2).

Table 1
CO_2 adsorption and desorption conditions used in the thermogravimetric analyzer for testing biowaste-based adsorbents without lanthanum functionalization.

Process	Atmosphere	Temperature (°C)	Duration (min)
Desorption	N_2	120	30
Cooling ramp	N_2	120—30	9
Adsorption	CO_2	30	60
Heating ramp	N_2	30—120	9

Table 2
CO_2 adsorption and desorption conditions used in the thermogravimetric analyzer for testing biowaste-based adsorbents with lanthanum functionalization.

Process	Atmosphere	Temperature (°C)	Duration (min)
Desorption	N_2	200	30
Cooling ramp	N_2	200—30	17
Adsorption	CO_2	30	60
Heating ramp	N_2	30—200	17

$$q_t = \frac{1000 \bullet m_i + \Delta m_t - m_{min}}{m_i}, m_{min} = (1000 \bullet m_i + \Delta m)_{min} \quad (2)$$

where m_i corresponds to the initial adsorbent mass (g), Δm_t to the mass variation (g) given by TGA for each time and m_{min} corresponds to the mass of regenerated adsorbent (g) determined as the baseline of minimum mass for each cycle. The carrying capacity of tested adsorbents was determined and compared using a pure CO_2 stream and a real flue gas stream provided by an industrial partner. Note that using real gas allowed to determine the impact of other impurities (e.g., CO and SO_2) on CO_2 capture performance of tested adsorbents. The composition of the flue gas is presented in Table 3.

3. Results and discussion

3.1. Biowaste-adsorbent preparation and surface characterization

Table 4 shows the char yields obtained for tested biowaste precursors using pyrolysis and HTC. The results indicated that HTC's yield was higher than the pyrolysis' for all the biowaste precursors. The yields were determined based on multiple batches, with standard deviations below 3 % for pyrolysis and 7 % for HTC. Pyrolysis and HTC yields obtained for both rice husk and grape marc were similar to the ones found in the literature for slow pyrolysis (~35 %) (Singh et al., 2019) and food waste-based hydrochars (43—66 %), respectively. The yield of the cork pyrolysis is consistent with a proximate analysis presented in the literature for this material (Montero et al., 2014); as the fixed carbon and ash contents are lower than the grape marc's and rice husk's (Deiana et al., 2014; Qi et al., 2019). On the other hand, the higher yield of cork in HTC can be explained by its high content of suberin (33–50 % by mass), which confers cork high thermal resistance and low water absorption (Engel et al., 2022), potentially inhibiting the hydrolyzation that usually takes place during HTC.

Table 3
Flue gas composition used in CO_2 adsorption/desorption studies. Data provided by an industrial partner.

Flue gas component	Composition
O_2 (%)	11.7 ± 0.6
CO_2 (%)	15.4 ± 0.9
CO (ppm)	839 ± 42
SO_2 (ppm)	3.8 ± 0.2
H_2O (ppm)	645[a]
NO_x (ppm)	< 1.0[b]

[a] *Quantified at the Flue Gas bottle exit using an Aspen Plus flash model (UNIFAC physical property method).*
[b] *Below the quantification limit of the analyzer.*

Table 4
Yields of the char production using grape marc, rice husk and cork stoppers.

Precursor	Yield (%) *Pyrolysis*	*Hydrothermal carbonization*
Grape marc	33.5	65.3
Rice husk	37.2	61.8
Cork stoppers	20.7	86.8

XRD and FTIR results are presented in Fig. 2 and Fig. 3, respectively. The crystalline structures of all carbon-based materials synthetized from the different biowaste precursors via pyrolysis and HTC exhibit the characteristic broad and asymmetric peak at ~ 22°2θ. This peak corresponds to the lattice spacing of C (002) in highly disordered materials, as reported in previous studies (Ismail et al., 2020; Wang et al., 2022; Casal et al., 2023). Moreover, some adsorbent samples display a weak diffraction peak at ~ 43°2θ, attributed to the presence of (101) reflection planes within partially graphitized carbon structures (Ismail et al., 2020; Casal et al., 2023). In addition to the C (002) and (101) crystalline planes, the adsorbent samples obtained from grape biowaste exhibits the crystalline structure corresponding to calcium carbonate (ICDD: 01–086-2340) and lanthanum oxide carbonate (ICDD: 01–084-1964). Similar findings were reported by Frikha et al. (Frikha et al., 2021), who in addition stated that calcium ranks among the predominant mineral components within grape biomass. X-ray diffraction patterns also indicated the existence of lanthanum oxide (ICDD: 03–065-3185) on the material's surface. Regarding the cork samples, the crystalline phase ascribed to calcium carbonate (ICDD: 01–086-2340) was identified in one sample. It is convenient to highlight that calcium is one of the principal elements found in cork stoppers, which in addition contain significant quantities of Si, S, Cl and K (dos Santos et al., 2013; Debastiani et al., 2021). Lanthanum moieties, specifically lanthanum hydroxide (ICDD: 00–006-0585), lanthanum carbonate hydrate (ICDD: 00–025-1400), and lanthanum carbonate hydroxide hydrate (ICDD: 00–046-0386), were identified in carbonized samples, while the diffraction peaks observed at ~ 13.1, 15.4, 21.4, 23.8 and 35.5°2θ can be attributed to silicon oxide. The existence of this last compound stems from the external treatment of cork stoppers with silicon resins, which is employed to enhance the sealing characteristics of cork materials (Debastiani et al., 2021). Finally, all adsorbent prepared from rice husk display the distinct diffraction peak corresponding to the organic crystalline compounds, linked to the C (002) crystalline plane of carbon-base materials at ~ 21.5°2θ (Wang et al., 2022). Furthermore, the crystalline structure of lanthanum hydroxide (ICDD: 00–036-1481) was identified in the adsorbent samples.

On the other hand, FTIR spectra of all the biowaste-based adsorbents exhibit absorption bands ascribed to stretching vibration of O–H (~3440 cm^{-1}) and C–H (2920 and 2850 cm^{-1}) bonds, respectively (Quang et al., 2022; Domingos et al., 2024). Additional features include stretching vibrations associated with O-C=O (1735, 1280 and 1175 cm^{-1}), C=O (~1750 – 1625 cm^{-1}), C=C (~1560 – 1460 cm^{-1}), C-O-C (~1400 and 1065 cm^{-1}), C-O (~1380 – 1100 cm^{-1}), C–H (1100 and 800 cm^{-1}), C–C–O (~880 cm^{-1}), C=H (~850 – 750 cm^{-1}), and aromatic rings (~900 – 700 cm^{-1}), besides rocking vibration band of CH_2 (740 cm^{-1}) (Wang et al., 2022; Domingos et al., 2024; del Pozo et al., 2022; Gong et al., 2024; Apolloni et al., 2025; García-Laynez et al., 2025; Rezvani et al., 2025). Rice husk-derived adsorbents exhibit distinctive absorption bands associated with the asymmetric stretching vibrations of Si–O–Si (~800 and 476 cm^{-1}) reflecting the presence of silica (Apolloni et al., 2025; Rezvani et al., 2025; da Rocha and de G, Santana Junior MB, Pier Macuvele DL, Riella HG, Ienczak JL, Padoin N, , 2025). In the lanthanum functionalized adsorbents, the stretching vibration of La-O bond can be identified at ~ 1454, 850, 675 and/or 465 cm^{-1} (Li et al., 2020; Kumar et al., 2019).

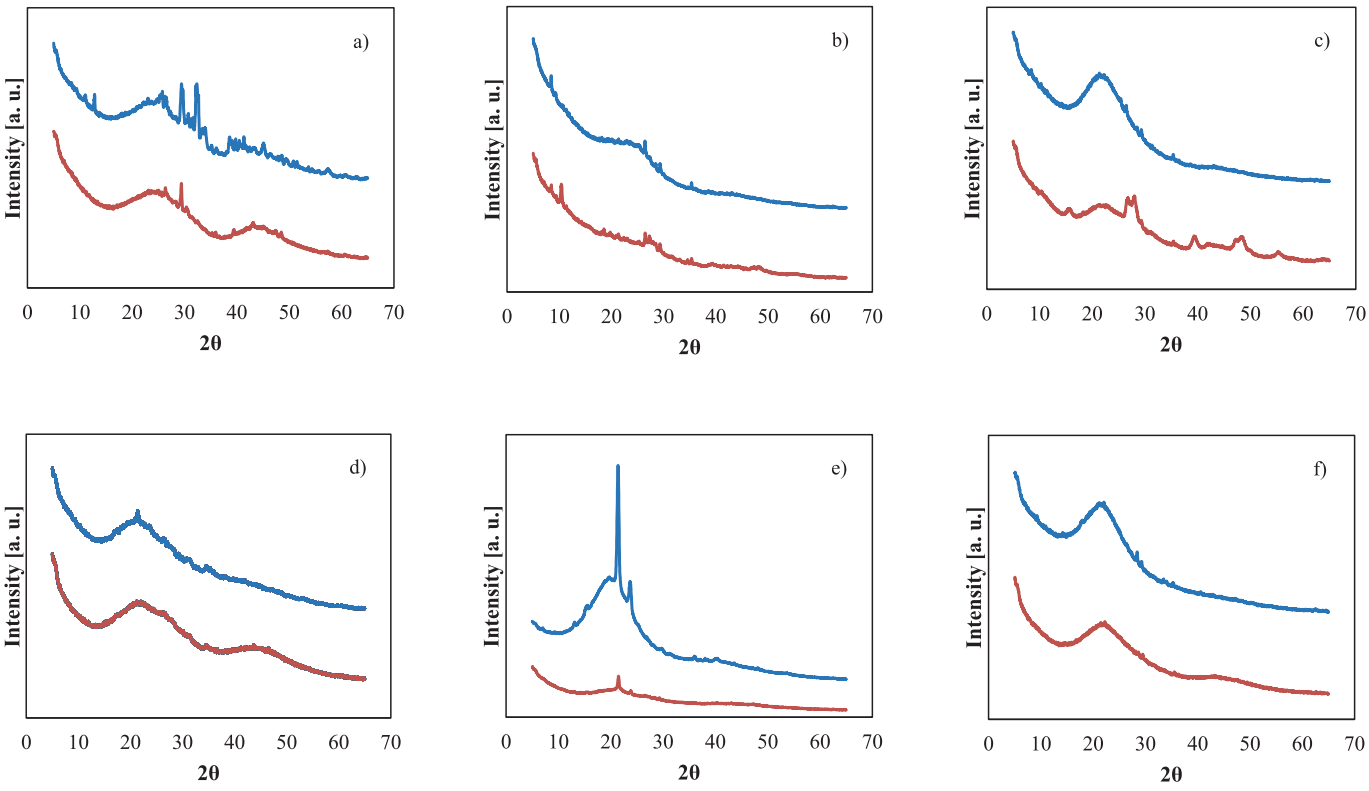

Fig. 2. XRD results of CO_2 capturing adsorbents obtained via a,b,c) pyrolysis and d,e,f) hydrothermal carbonization. Biowaste precursor: a,d) grape marc, b,e) cork stoppers and c,f) rice husk. The red and blue curves correspond to adsorbents with and without lanthanum functionalization, respectively.

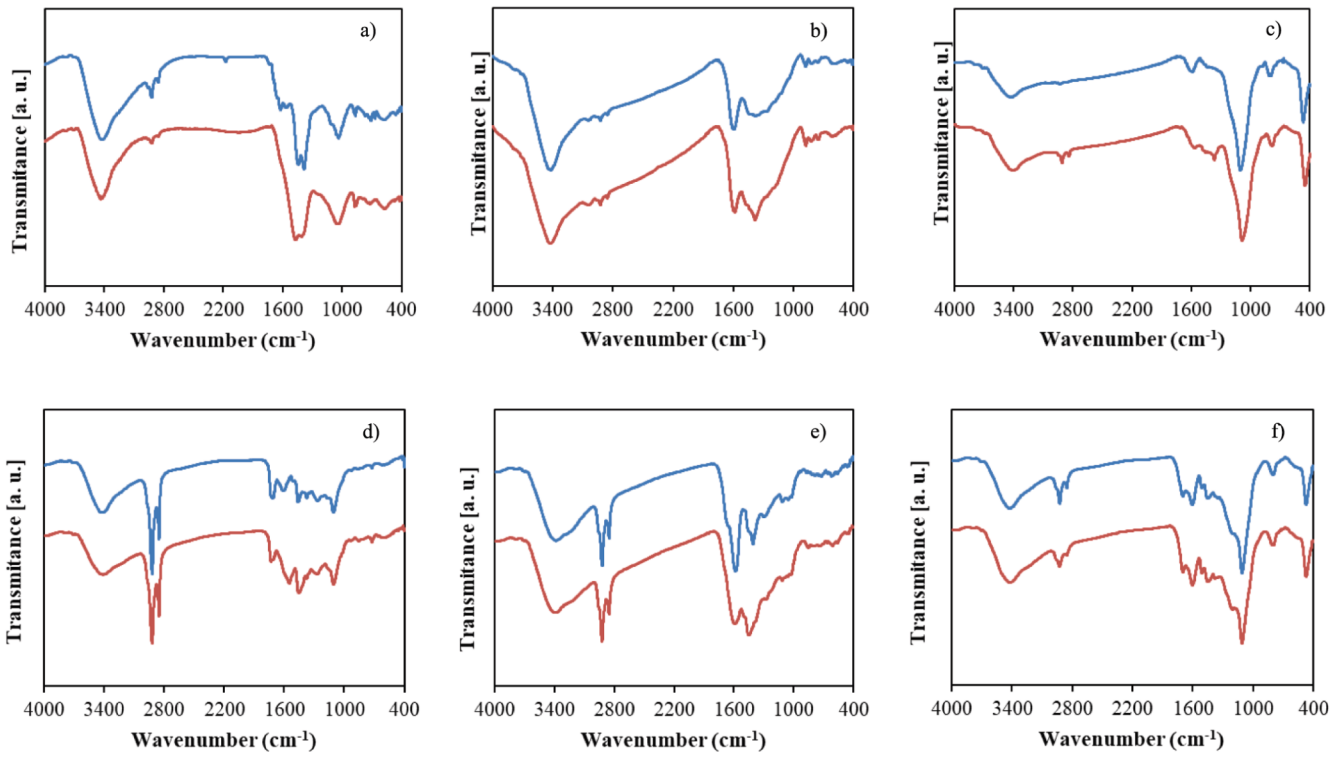

Fig. 3. FTIR results of the CO_2 capturing adsorbents obtained via a,b,c) pyrolysis and d,e,f) hydrothermal carbonization. Biowaste precursor: a,d) grape marc, b,e) cork stoppers, and c,f) rice husk. The red and blue curves correspond to adsorbents with and without lanthanum functionalization, respectively.

Although the adsorbents obtained by both carbonization routes share several common surface functional groups, the overall intensity of

adsorption bands of spectra from hydrochars is generally higher than those for pyrolyzed materials. This result indicates a higher concentration or abundance of surface functional groups generated during HTC-based carbonization process. The functional groups identified in cork-based adsorbents primarily originate from suberin (the main structural component), polysaccharides and lignin (Wang et al., 2022; Gong et al., 2024), while those in rice husk-based adsorbents are mainly contributed by cellulose, hemicellulose, lignin and silicon dioxide (da Rocha and de G, Santana Junior MB, Pier Macuvele DL, Riella HG, Ienczak JL, Padoin N, , 2025). For adsorbents synthesized from grape marc biowaste, the functional groups are predominantly derived from cellulose, hemicellulose, and lignin (Titone et al., 2025).

Scanning electron microscopy (SEM) micrographs of selected samples are reported in Fig. 4. The hydrochar surface exhibits a well-organized structure with some pores containing small aggregates, while the micrograph of the pyrolyzed grape marc shows a homogeneous and porous structure, resulting from the degradation of organic matter and the release of volatile compounds during thermal treatment. After functionalization with lanthanum, the hydrochar surface becomes irregular and non-homogeneous, suggesting that the pores were clogged with lanthanum flakes deposited on the surface. In contrast, the pyrolyzed material preserves its well-developed porous structure, and lanthanum is detected dispersed on the adsorbent surface. This result suggests that the incorporation of lanthanum does not collapse the pore network.

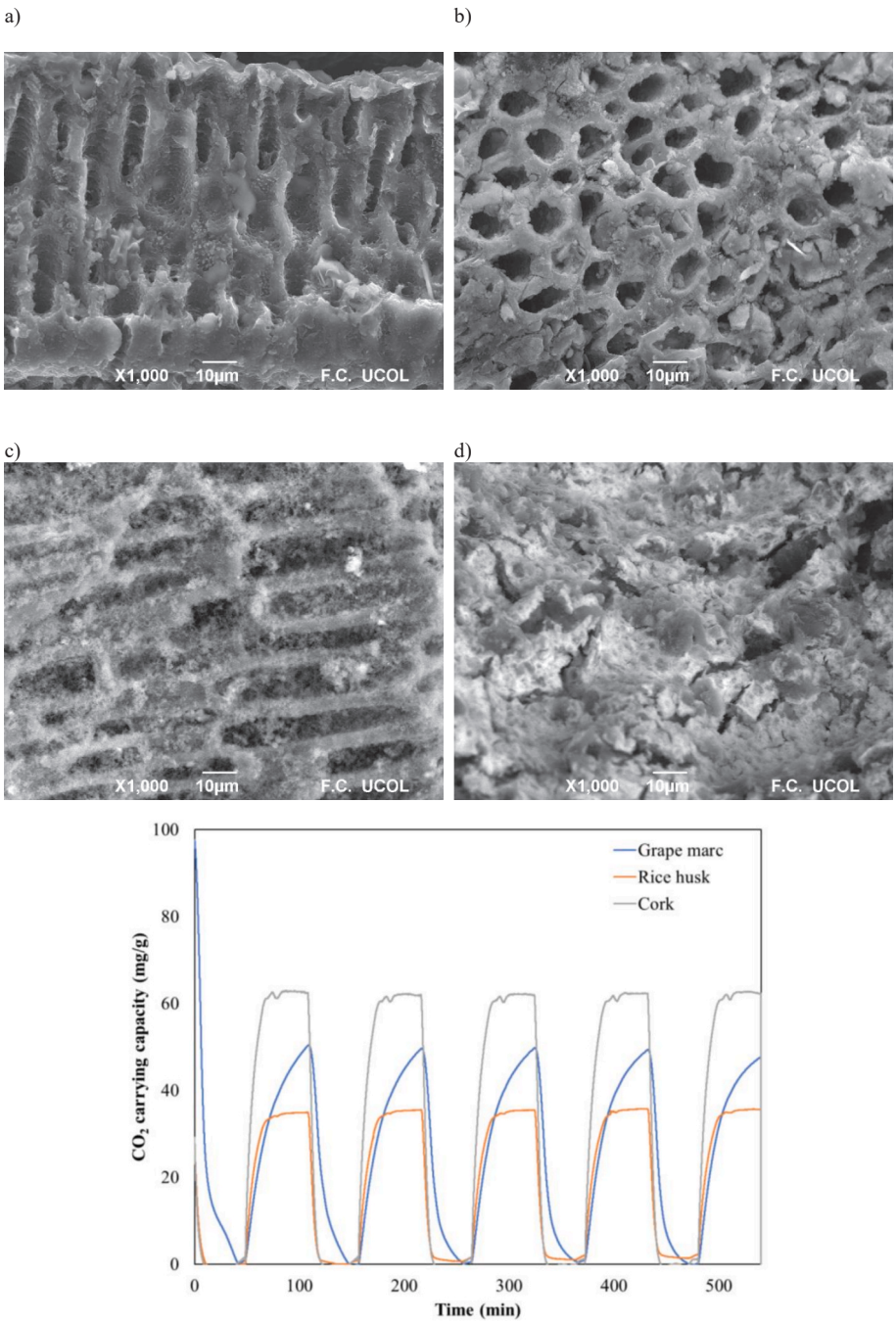

Fig. 4. Raw (a,c) and lanthanum-functionalized (b,d) adsorbents obtained by pyrolysis (a,b) and hydrothermal carbonization (c,d) of grape marc. Fig. 4. The multicyclic activity of biowaste-based adsorbents obtained via pyrolysis for CO_2 capture (1 data point per second). The desorption was performed at 120 °C in an inert atmosphere and the adsorption at 30 °C under CO_2 flow.

3.2. CO_2 capture performance

The multicyclic carrying capacity of the adsorbents obtained via pyrolysis without or with lanthanum functionalization is represented in Fig. 4 and Fig. 5, respectively, while Fig. 6 and Fig. 7 report the performance of hydrochars without and with lanthanum functionalization, respectively. The raw data of the TGA runs used for obtaining the multicyclic carrying capacity of the adsorbents is presented in Appendix A. Overall, HTC process leads to adsorbents with lower carrying capacity than the ones obtained via pyrolysis. The adsorbents produced from HTC show lower surface area, but more functional groups than biochars. Specifically, the surface area of synthetized adsorbents via pyrolysis from grape marc, rice husk and cork stoppers was 22, 9 and 5 m^2/g, respectively. In comparison, their counterparts obtained through hydrothermal carbonization exhibited surface areas lower than 5 m^2/g. Therefore, the lower CO_2 capturing activity of the hydrochars is related to their low porosity where physisorption is expected to govern the separation process (Cognigni et al., 2025). Overall, lanthanum functionalization does not show a significant improvement in CO_2 capture, which can be attributed to the reduction in surface area, probably due to partial pore blockage by the lanthanum species deposited on the surface. Specifically, the surface area available for gas adsorption decreased up to 30–35 % for pyrolyzed adsorbents, and for hydrochars it was less than 1 m^2/g. However, the adsorption kinetics of the grape marc-based adsorbents were different where the sample functionalized with lanthanum exhibited a faster kinetics. Note that the grape marc adsorbent showed a total pore volume of 0.0252 cm^3/g and a micropore volume of 0.003 cm^3/g. Therefore, this material had mesopores and also low microporosity.

The carrying capacities obtained in this study are lower than some of the ones reported in the literature (Li et al., 2025; Quan et al., 2023), which could be improved by adding an activation step, for example with KOH. However, it is important to highlight the maintenance of biowaste-based adsorbent activity over consecutive adsorption/desorption cycles, which is interesting for future industrial implementation of the process. The adsorbent production via grape marc and cork stoppers pyrolysis seems to be an interesting topic for future studies.

The kinetic performance of biowaste-based adsorbents obtained from pyrolysis was modelled, which showed the most promising CO_2 capture results. This modelling considers that the variation of the occupied adsorbent active sites in the surface of theses biowaste-based

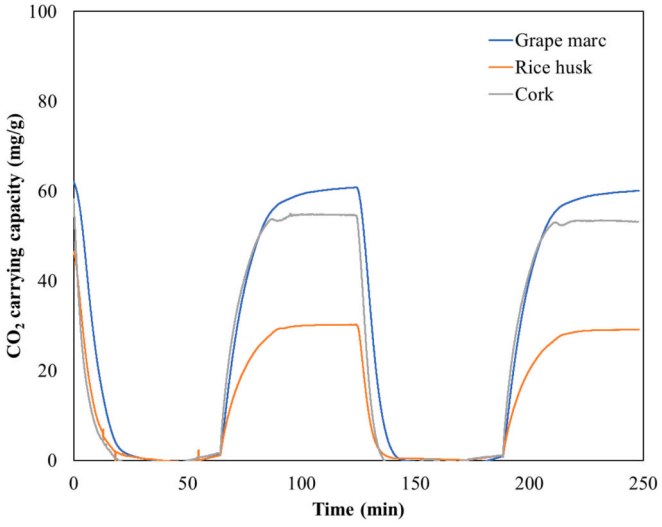

Fig. 5. The multicyclic activity of biowaste-based adsorbents obtained via pyrolysis and lanthanum functionalization for CO_2 capture (1 data point per second). The desorption was performed at 200 °C in an inert atmosphere and the adsorption at 30 °C under CO_2 flow.

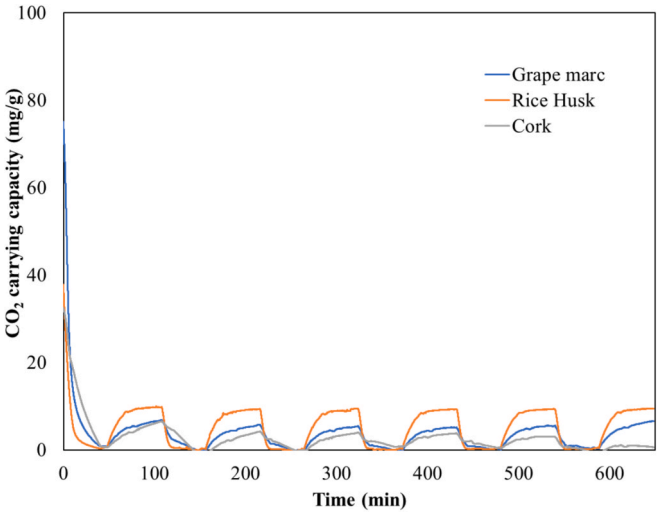

Fig. 6. The multicyclic activity of biowaste-based adsorbents obtained via hydrothermal carbonization for CO_2 capture (1 data point per second). The desorption was performed at 120 °C in an inert atmosphere and the adsorption at 30 °C under CO_2 flow.

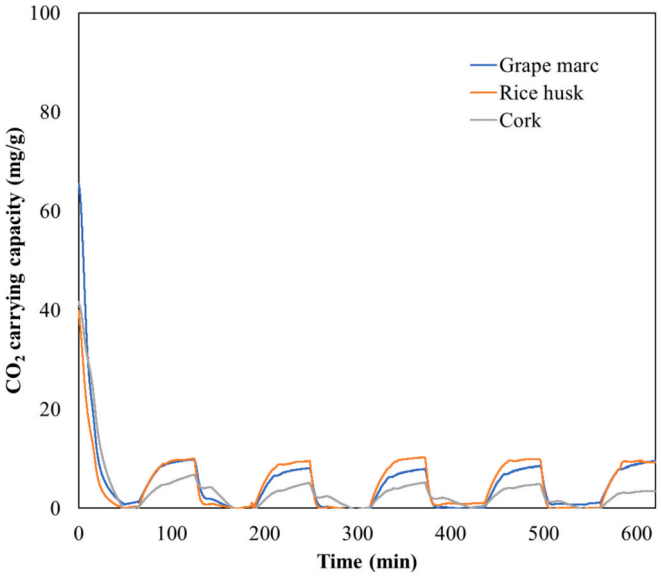

Fig. 7. The multicyclic activity of biowaste-based adsorbents obtained via hydrothermal carbonization and lanthanum functionalization for CO_2 capture (1 data point per second). The desorption was performed at 200 °C in an inert atmosphere and the adsorption at 30 °C under CO_2 flow.

materials with time, $\frac{d\theta_t}{dt}$, is given by a trade–off between the adsorption rate (r_a) and the desorption rate (r_d), as described by Equation (3).

$$\frac{d\theta_t}{dt} = r_a - r_d \tag{3}$$

It was assumed the adsorption followed a first-order kinetics regarding CO_2 concentration in the gas (C_t) and regarding the fraction of free active sites in the adsorbent surface $(1-\theta_t)$. On the other hand, the desorption kinetic was assumed to follow a first-order kinetics with respect to the occupied sites in the adsorbent surface (θ_t). The kinetic rates of adsorption and desorption are given in Equations (4) and (5), respectively,

$$r_a = k_a C_t (1-\theta_t) \tag{4}$$

$$r_d = k_d\theta_t \tag{5}$$

$$\frac{d\theta_t}{dt} = k_aC_t(1-\theta_t) - k_d\theta_t \tag{6}$$

$$\theta_t = \frac{q_t}{q_{max}} \Rightarrow \frac{dq_t}{dt} = k_aC_t(q_{max}-q_t) - k_dq_t \tag{7}$$

where k_a is the adsorption kinetic constant and k_b the desorption kinetic constant. The variation of the fraction of occupied sites in the adsorbent's surface with time t is thus given by Equation (6) and the variation of the CO_2 captured by the adsorbent (q_t) is given by Equation (7), in which q_{max} corresponds to the maximum CO_2 carrying capacity of the adsorbent. To model the CO_2 carrying capacity with time, the carrying capacity is integrated between 0 and q_t and the time between 0 and t, as presented in Equation (8).

$$\int_0^{q_t} \frac{dq_t}{k_aC_t(q_{max}-q_t) - k_dq_t} = \int_0^t dt \tag{8}$$

Concerning the adsorption process from a pure CO_2 stream, the CO_2 concentration in the stream remains unchanged after capture and equals the initial CO_2 concentration (C_0). The carrying capacity variation with time is thus given by Equation (9).

$$q_t = \frac{k_aC_0q_{max}}{k_aC_0 + k_d}(1 - \exp(-(k_aC_0 + k_d)t)) \tag{9}$$

The deduction of this equation is presented in Appendix B of the Supplementary Material. Therefore, the CO_2 capture by the adsorbent follows a pseudo-first order kinetics, given by Equation (10), with $q_e = \frac{k_aC_0q_{max}}{k_aC_0+k_d}$ and $k_1 = k_aC_0 + k_d$.

$$q_t = q_e(1-\exp(-k_1t)), q_e = \frac{k_aC_0q_{max}}{k_aC_0+k_d}, k_1 = k_aC_0 + k_d \tag{10}$$

A pseudo-second order kinetics regarding the fraction of free sites on the adsorbent surface, given by Equations (11) and (12), was also tested.

$$\frac{dq_t}{dt} = k_2(q_e - q_t)^2 \tag{11}$$

$$q_t = \frac{q_et}{\frac{1}{q_ek_2} + t} \tag{12}$$

The modeling results for the pseudo-first order and pseudo-second order adsorption kinetics for the adsorbents obtained via pyrolysis, with and without lanthanum functionalization, is presented in Table 5. Note that these results were obtained by minimizing the sum of squares error of all the adsorption cycles where the joint minimization was possible since no deactivation was present among the cycles. The mean squared error (MSE) obtained using a pseudo-first order kinetics is lower than using a pseudo-second order kinetics for all the analyzed samples, see Table 5. Therefore, it is possible to conclude that a pseudo-first order kinetics is best suited to describe CO_2 capture performance of all the adsorbents obtained via pyrolysis with and without lanthanum functionalization.

It was assumed the maximum carrying capacity was achieved at the end of the adsorption steps. Therefore, the desorption steps were modelled by integrating q_t in Equation (7) between q_{max} and q_t, as presented in Equation (13).

$$\int_{q_{max}}^{q_t} \frac{dq_t}{k_aC_t(q_{max}-q_t) - k_dq_t} = \int_0^t dt \tag{13}$$

As the desorption was performed in the presence of a pure nitrogen stream, the CO_2 concentration in the gas stream (C_t) was zero resulting in Equation (14), whose deduction is presented in the Appendix C of the Supplementary Material.

Table 5
Kinetic constants using pseudo first order and pseudo second order approaches for the modelling of CO_2 capture using biowaste-based adsorbents obtained via pyrolysis.

Adsorbent sample		Adsorption			
Precursor	Preparation route	Parameter	Pseudo 1st order kinetics	Pseudo 2nd order kinetics	Units
Grape marc	Pyrolysis	k_n	$7.48{\cdot}10^{-4}$	$8.00{\cdot}10^{-6}$	$(g/mg)^{n-1}{\cdot}s^{-1}$
		q_e	56.05	77.44	$mg/g_{adsorbent}$
		MSE	0.39	0.62	$(mg/g_{adsorbent})^2$
Cork	Pyrolysis	k_n	$2.39{\cdot}10^{-3}$	$4.66{\cdot}10^{-5}$	$(g/mg)^{n-1}{\cdot}s^{-1}$
		q_e	62.77	70.83	$mg/g_{adsorbent}$
		MSE	0.80	6.03	$(mg/g_{adsorbent})^2$
Rice husk	Pyrolysis	k_n	$2.09{\cdot}10^{-3}$	$6.70{\cdot}10^{-5}$	$(g/mg)^{n-1}{\cdot}s^{-1}$
		q_e	35.36	40.60	$mg/g_{adsorbent}$
		MSE	0.25	1.89	$(mg/g_{adsorbent})^2$
Grape marc	Pyrolysis + La	k_n	$1.56{\cdot}10^{-3}$	$2.37{\cdot}10^{-5}$	$(g/mg)^{n-1}{\cdot}s^{-1}$
		q_e	61.38	73.84	$mg/g_{adsorbent}$
		MSE	0.87	5.64	$(mg/g_{adsorbent})^2$
Cork	Pyrolysis + La	k_n	$2.14{\cdot}10^{-3}$	$4.53{\cdot}10^{-5}$	$(g/mg)^{n-1}{\cdot}s^{-1}$
		q_e	54.9	62.80	$mg/g_{adsorbent}$
		MSE	0.59	4.59	$(mg/g_{adsorbent})^2$
Rice husk	Pyrolysis + La	k_n	$1.73{\cdot}10^{-3}$	$5.87{\cdot}10^{-5}$	$(g/mg)^{n-1}{\cdot}s^{-1}$
		q_e	30.38	35.75	$mg/g_{adsorbent}$
		MSE	0.31	1.24	$(mg/g_{adsorbent})^2$

MSE: Mean Squared Error.
n: Order of Reaction

$$q_t = q_{max} \bullet \exp(-k_dt) \tag{14}$$

The calculated values of the adsorption and desorption kinetic constants and the maximum carrying capacity are presented in Table 6 for all the pyrolyzed biowaste-based adsorbents. The fitting of the experimental results of the adsorption and desorption with the pseudo first order kinetics parameters shown in Table 6 is represented in the Appendix D of the Supplementary Material. It is possible to conclude the La-functionalization improves the kinetic performance and the maximum adsorption capacity of the grape marc-based adsorbent.

Table 6
Calculated values of pseudo first order kinetic constant (k_1) and maximum carrying capacity (q_e) of biowaste-based adsorbents obtained from pyrolysis.

Adsorbent sample		Adsorption		Desorption	
Precursor	Preparation route	$k_1(s^{-1})$	q_e(mg/g)	$k_d(s^{-1})$	q_{max}(mg/g)
Grape marc	Pyrolysis	$7.48{\cdot}10^{-4}$	56.05	$2.10{\cdot}10^{-3}$	46.10
	Pyrolysis + La	$1.56{\cdot}10^{-3}$	61.38	$3.24{\cdot}10^{-3}$	64.24
Cork	Pyrolysis	$2.39{\cdot}10^{-3}$	62.77	$4.92{\cdot}10^{-3}$	65.13
	Pyrolysis + La	$2.14{\cdot}10^{-3}$	54.97	$4.79{\cdot}10^{-3}$	57.78
Rice husk	Pyrolysis	$2.09{\cdot}10^{-3}$	35.36	$4.34{\cdot}10^{-3}$	35.12
	Pyrolysis + La	$1.73{\cdot}10^{-3}$	30.38	$4.39{\cdot}10^{-3}$	31.80

3.3. Effect of the desorption time and temperature on CO_2 capture

The effect of the desorption time on the adsorption capacity of the pyrolyzed grape marc sample was evaluated by increasing the desorption time from 30 min to 1 h, as represented in Fig. 8. The experimental carrying capacity obtained with a longer desorption time was slightly lower than when the desorption lasted 30 min. This suggests the deviation falls into the error of the analysis and that a desorption time of 30 min is enough to fully desorb CO_2 from the adsorbent's surface.

On the other hand, the effect of the temperature on the relative desorption of the functionalized and non–functionalized grape marc-based adsorbents was evaluated by increasing the temperature from 120 to 200 °C and the results are presented in Table 7. The relative desorption increases with the increase of temperature for the grape marc-based adsorbents, leading to major availability of sample's pores and, therefore, on the maximum carrying capacity. This enhances the kinetic performance of the adsorbent in the following adsorption step, as represented in Fig. 9 and Fig. 10 for non–functionalized and La–functionalized grape marc-based adsorbent, respectively. The relative desorption of the La–functionalized grape marc-based adsorbent is lower than the non-functionalized one, which suggests the lanthanum functionalization decreases the porosity of the sample, as already confirmed by adsorbent characterization results.

Although a good correlation was found for grape marc adsorption using a pseudo first-order kinetics (Table 5), with the increase of the adsorption time (Fig. 9), it is possible to notice that the CO_2 adsorption does not stabilize at q_e (56.06 mg/g) as predicted by the model for the non-functionalized grape marc–based sample. This result was consistent with the presence of microporosity within the sample obtained from nitrogen physisorption, which is also in line with the reported porosity of grape-marc based adsorbents in other studies (Frikha et al., 2021). In this case, the CO_2 adsorption by the adsorbent is the sum of the CO_2 adsorbed on the micropores (μ) and on the mesopores (m), each showing a different adsorption rate in the form given by Equation (10). Therefore, the resulting carrying capacity is given by Equation (15).

$$q_t = q_{e,m} \bullet (1 - \exp(-k_{1,m}t)) + q_{e,\mu} \bullet (1 - \exp(-k_{1,\mu}t)) \quad (15)$$

The calculated adsorption kinetics constants and the maximum carrying capacity are presented in Table 8 for non-functionalized and La-functionalized grape marc-based adsorbent samples at the studied temperatures. It is possible to notice that the MSE is significantly reduced when using Equation (15) to describe the kinetics of the non-functionalized adsorbent. The results also shows that $q_{e,\mu} < q_{e,m}$ suggesting that adsorbent microporosity played a secondary role for CO_2 adsorption on this adsorbent. On the other hand, the MSE of the La-functionalized adsorbent indicates that Equation (10) presents a good fit for the adsorption data obtained, which suggests the adsorbent loses its microporosity on the functionalization step. These findings agreed with the adsorbent characterization results reported above.

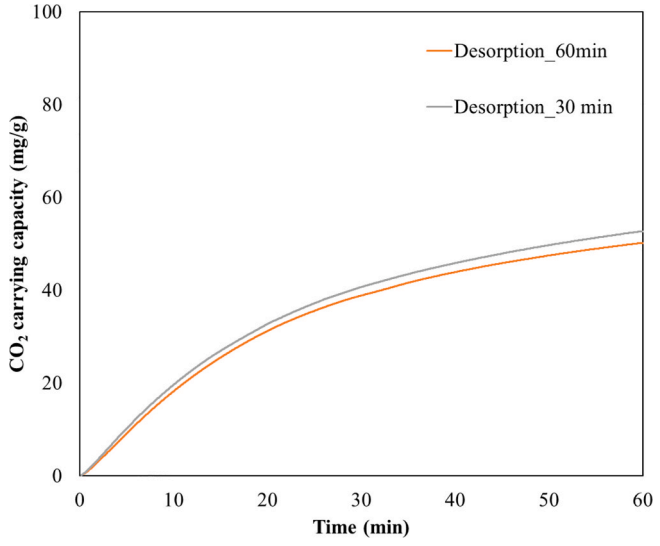

Fig. 8. Effect of the desorption time on the 1st cycle experimental carrying capacity of the adsorbent obtained by pyrolysis of grape marc.

Table 7
CO_2 desorption of the grape marc-based adsorbents at 120, 150 and 200 °C.

Adsorbent preparation	Desorption, °C	m_i(mg)	m_{min}(mg)	Relative desorption (%)
Pyrolysis	120	12.27	10.98	10.5
Pyrolysis	150	18.64	16.49	11.5
Pyrolysis	200	13.08	11.52	12.0
Pyrolysis + La	120	15.64	14.67	6.22
Pyrolysis + La	200	13.67	12.81	6.30

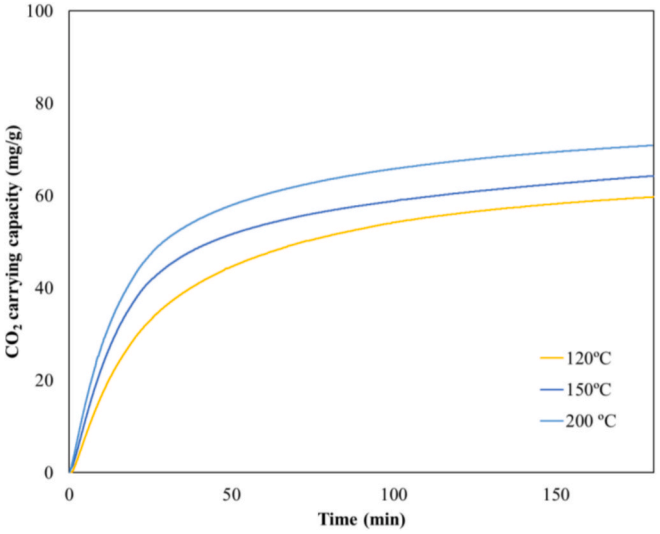

Fig. 9. Effect of the desorption temperature on the 1st cycle experimental carrying capacity of the adsorbent obtained by pyrolysis of grape marc.

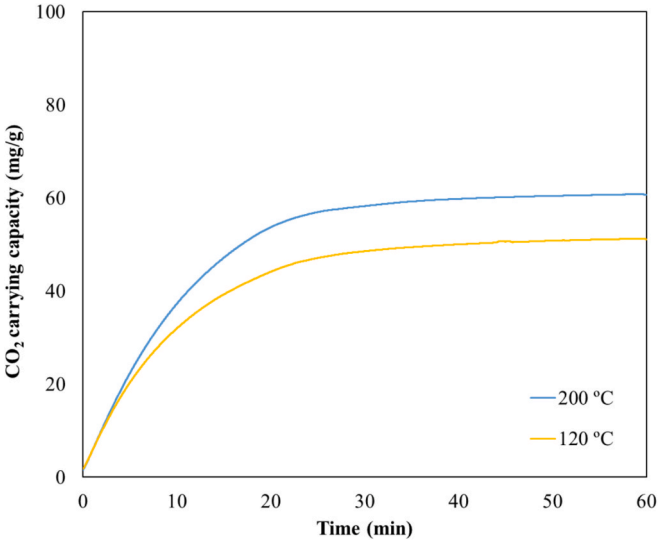

Fig. 10. Effect of the desorption temperature on the 1st cycle experimental carrying capacity of the adsorbent obtained by pyrolysis of grape marc and functionalized with lanthanum.

Table 8
Calculated adsorption kinetic constant and maximum adsorption capacity of the mesopores and micropores of grape marc-based adsorbents under desorption temperature between 120 and 200 °C.

Adsorbent preparation	Desorption temperature (°C)	Kinetic considered	Mesopores $k_{1,m}(s^{-1})$	$q_{e,m}$(mg/g)	Micropores $k_{1,\mu}(s^{-1})$	$q_{e,\mu}$(mg/g)	MSE ((mg/g)^2)
Pyrolysis	120	Eq. (10)	$5.10 \cdot 10^{-4}$	57.91	–	–	1.65
		Eq. (15)	$7.69 \cdot 10^{-4}$	41.45	$1.13 \cdot 10^{-4}$	26.19	0.17
	150	Eq. (10)	$6.87 \cdot 10^{-4}$	61.12	–	–	3.24
		Eq. (15)	$1.02 \cdot 10^{-3}$	47.56	$0.97 \cdot 10^{-4}$	25.69	0.19
	200	Eq. (10)	$7.36 \cdot 10^{-4}$	67.72	–	–	4.09
		Eq. (15)	$1.15 \cdot 10^{-3}$	51.20	$1.36 \cdot 10^{-4}$	25.84	0.09
Pyrolysis + La	120	Eq. (10)	$1.65 \cdot 10^{-3}$	51.13	–	–	0.08
	200	Eq. (10)	$1.61 \cdot 10^{-3}$	61.31	–	–	0.44

MSE: Mean Squared Error.
Eq: Equation

Regarding the adsorption on the mesopores, both $q_{e,m}$ and $k_{1,m}$ increase with the increase of temperature for the non-functionalized samples, which is related to the availability of adsorption sites caused by a more effective desorption. On the other hand, the desorption temperature does not play an important role in the calculated micropores constants $k_{1,\mu}$ and $q_{e,\mu}$, which suggest full desorption is obtained within the micropores at 120 °C.

3.4. Capturing CO_2 from flue gas

The flue gas has lower CO_2 partial pressure (15.4 %, Table 3), which leads to lower CO_2 adsorption rate and maximum adsorption capacity of the adsorbent, considering the same total gas flowrate. CO_2 capture using the real flue gas from a cement plant is reported in Fig. 11, Fig. 12 and Fig. 13 for adsorbents obtained from the pyrolysis of grape marc, cork stoppers and rice husk, respectively, while the capture performance of the corresponding La-functionalized adsorbents is presented in Fig. 14, Fig. 15, and Fig. 16, respectively.

Since the cement plant flue gas stream is not fully composed of CO_2, the concentration of CO_2 at the exit of the thermogravimetric analyzer ($C_{f,t}$) increases over time with the decrease of the CO_2 capturing rate ($r_{CO_2,cap,t}$) following Equation (16).

$$C_{f,t} = C_o x_{CO_2,f,t}, x_{CO_2,f,t} = \frac{F_{CO_2,i} - r_{CO_2,cap,t}}{F_{CO_2,i} - r_{CO_2,cap,t} + F_{inert}}, = r_{CO_2,cap,t} = \frac{m_{char}\frac{dq_t}{dt}}{M_{w,CO_2}} \quad (16)$$

Thus, to obtain a suitable representation of the adsorption kinetics when using flue gas, Equation (7) must be integrated considering the variation of CO_2 concentration at the exit of the reactor. To understand the impact of the variation in the CO_2 concentration when estimating the kinetics of

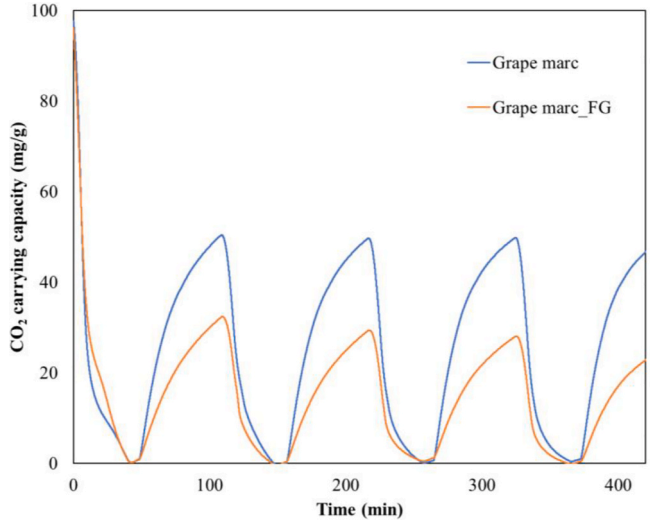

Fig. 11. Effect of using real cement plant flue gas on the multicyclic activity of the adsorbent obtained by grape marc's pyrolysis. "FG" denotes flue gas.

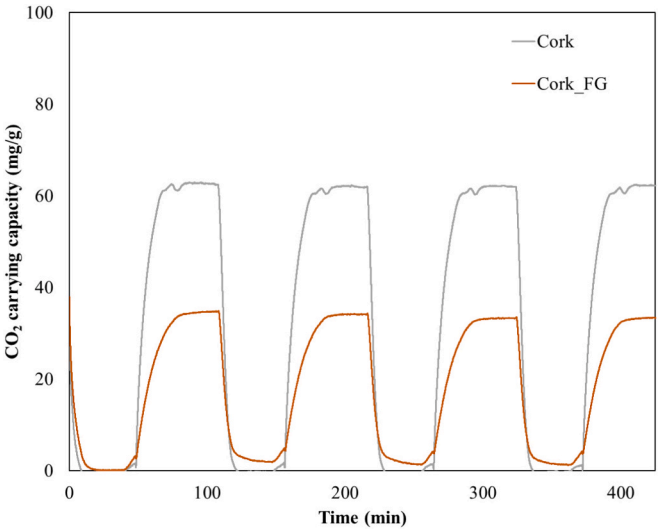

Fig. 12. Effect of using real cement plant flue gas on the multicyclic activity of the adsorbent obtained by cork stoppers' pyrolysis. "FG" denotes flue gas.

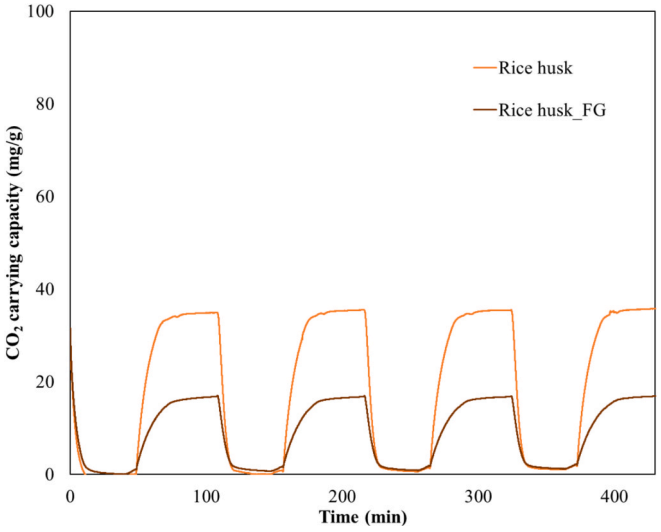

Fig. 13. Effect of using real cement plant flue gas on the multicyclic activity of the adsorbent obtained by rice husk's pyrolysis. "FG" denotes flue gas.

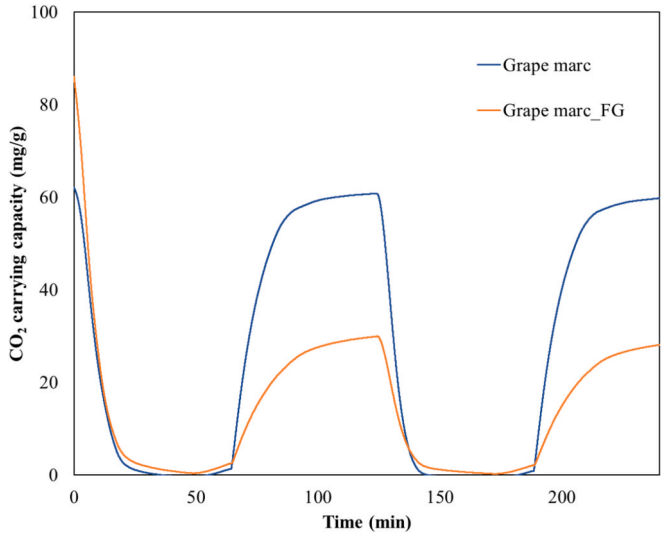

Fig. 14. Effect of using real cement plant flue gas on the multicyclic activity of the adsorbent obtained by grape marc's pyrolysis and functionalized with lanthanum. "FG" denotes flue gas.

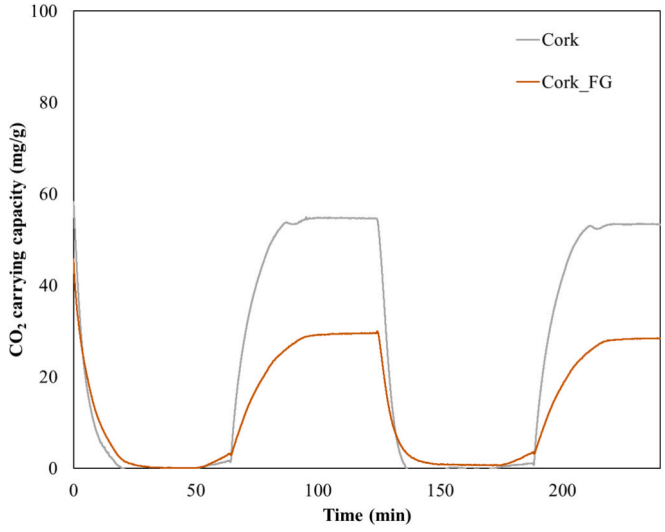

Fig. 15. Effect of using real cement plant flue gas on the multicyclic activity of the adsorbent obtained by cork's pyrolysis and functionalized with lanthanum. "FG" denotes flue gas.

the reaction, cork-based adsorbent was analyzed, since it was the one which presented the highest kinetic rate, thus contributing to the highest variation in the flue gas composition. CO_2 capturing rate of this adsorbent in the kinetic-limited region was estimated based on the experimental data at $3.93{\cdot}10^{-5}$ $g_{CO2}/g_{adsorbent}/s$. The specific mass flowrate of CO_2 at the gas inlet stream when using flue gas is approximately 0.5 $g_{CO2}/g_{adsorbent}/s$, which led to a CO_2 composition of 15.4 % (v/v) at TGA exit (i.e., approximately equal to the gas feed composition). Therefore, the $C_{f,t}$ variation over time was considered negligible, allowing to estimate the adsorption capacity of the adsorbent by Equation (17).

$$q_t = q_{e,FG}\left(1 - e^{-k_{1,FG}t}\right), q_t = \frac{k_a C_{FG} q_{max}}{k_a C_{FG} + k_d}\left(1 - e^{-(k_a C_{FG} + k_d)t}\right), C_{FG} = C_o x_{CO_2,i} \tag{17}$$

The kinetic constants and maximum carrying capacities obtained from the experimental curves of each adsorbent using Equation (17) for

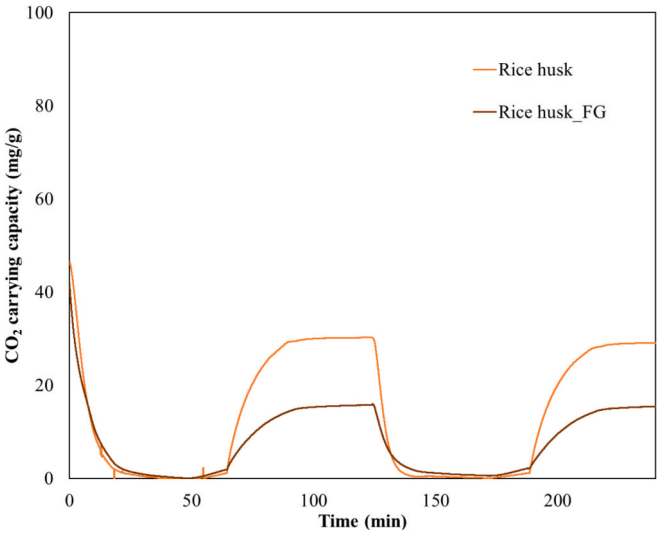

Fig. 16. Effect of using real cement plant flue gas on the multicyclic activity of the adsorbent obtained by rice husk's pyrolysis and functionalized with lanthanum. "FG" denotes flue gas.

adsorption and Equation (14) for desorption are presented in Table 9. No values are presented for grape marc-based adsorbent using flue gas and desorption temperature of 120 °C because the material presented deactivation over consecutive adsorption/desorption cycles. This suggests the desorption step was incomplete for this adsorbent using a flue gas stream.

Since the difference between the tests performed with biowaste-based adsorbents is only the flue gas, it should be possible to obtain k_a, k_d at 30 °C and q_{max} for each adsorbent, given k_1 and q_e values presented in Table 9. The adsorption and desorption constants at 30 °C were estimated according to Equation (18), whose deduction is presented in Appendix E of the Supplementary Material, and Equation (19), respectively, while q_{max} was given by Equation (20) using q_e obtained in the pure CO_2 experimental tests.

$$k_a = \frac{k_{1,CO_2} - k_{1,FG}}{C_0 - C_{FG}} \tag{18}$$

$$k_d = k_{1,CO_2} - k_a C_0 = k_{1,FG} - k_a C_{FG} \tag{19}$$

$$q_{max} = \frac{q_{e,CO_2}(C_0 k_a + k_d)}{C_0 k_a} \tag{20}$$

The estimated q_{max} was then used to calculate q_e that should be obtained using a flue gas stream with 15.4 % CO_2 (Equation (21)).

$$q_{e,FG} = \frac{q_{max} C_{FG} k_a}{C_{FG} k_a + k_d} \tag{21}$$

The estimated q_e values are presented in Table 10. It is possible to notice that the equilibrium adsorption capacity obtained experimentally is significantly higher than the adsorption capacity estimated using the CO_2 concentration in the stream. Therefore, the experimental and modelling results suggest that CO_2 is not the only gas component that is being adsorbed. Therefore, further tests are required to evaluate the selectivity of these materials and to understand the impact of each flue gas contaminant in CO_2 adsorption.

The first order adsorption kinetics (Equation (10)) was applied to each CO_2 adsorption cycle of pyrolyzed grape marc adsorbent using flue gas and desorption temperature of 120 °C. The kinetic constant was fitted for all the adsorption cycles, while the equilibrium carrying capacity was obtained for each cycle. The kinetic constant was estimated at $4.40{\cdot}10^{-4}$ s^{-1} and the equilibrium carrying capacity obtained for each

Table 9
Pseudo first-order adsorption kinetic constant (k_1), maximum carrying capacity (q_e), and deactivation kinetic constant (k_d) of CO_2 capture using biowaste-based adsorbents obtained via pyrolysis.

Biowaste	Inlet gas stream	Adsorbent preparation	Desorption temperature (°C)	Adsorption $k_1(s^{-1})$	q_e(mg/g)	Desorption $k_d(s^{-1})$	q_{max}(mg/g)
Grape marc	CO_2	Pyrolysis	120	$7.48{\cdot}10^{-4}$	56.05	$2.10{\cdot}10^{-3}$	46.10
Grape marc	Flue gas	Pyrolysis	120	*	*	*	*
Cork	CO_2	Pyrolysis	120	$2.39{\cdot}10^{-3}$	62.77	$4.92{\cdot}10^{-3}$	65.13
Cork	Flue gas	Pyrolysis	120	$1.49{\cdot}10^{-3}$	34.97	$3.25{\cdot}10^{-3}$	31.95
Rice husk	CO_2	Pyrolysis	120	$2.09{\cdot}10^{-3}$	35.36	$4.34{\cdot}10^{-3}$	35.12
Rice husk	Flue gas	Pyrolysis	120	$1.49{\cdot}10^{-3}$	16.90	$3.54{\cdot}10^{-3}$	15.77
Grape marc	CO_2	Pyrolysis + La	200	$1.61{\cdot}10^{-3}$	61.31	$3.24{\cdot}10^{-3}$	64.24
Grape marc	Flue gas	Pyrolysis + La	200	$9.42{\cdot}10^{-4}$	28.19	$2.51{\cdot}10^{-3}$	31.33
Cork	CO_2	Pyrolysis + La	200	$2.14{\cdot}10^{-3}$	54.97	$4.79{\cdot}10^{-3}$	57.78
Cork	Flue gas	Pyrolysis + La	200	$1.48{\cdot}10^{-3}$	29.73	$3.36{\cdot}10^{-3}$	31.23
Rice husk	CO_2	Pyrolysis + La	200	$1.73{\cdot}10^{-3}$	30.38	$4.39{\cdot}10^{-3}$	31.80
Rice husk	Flue gas	Pyrolysis + La	200	$1.41{\cdot}10^{-3}$	15.82	$2.30{\cdot}10^{-3}$	15.15

* The adsorption curves varied among the cycles. Therefore, the results are not presented in this table.

Table 10
Experimental and estimated equilibrium CO_2 capture using a flue gas stream.

Precursor	Adsorbent preparation	Desorption temperature (°C)	Experimental q_e(mg/g)	Estimated q_e(mg/g)
Cork	Pyrolysis	120	34.97	15.53
Rice husk	Pyrolysis	120	16.90	5.97
Grape marc	Pyrolysis + La	200	28.19	14.06
Cork	Pyrolysis + La	200	29.73	10.13
Rice husk	Pyrolysis + La	200	15.82	2.84

Table 11
Maximum equilibrium carrying capacity of pyrolyzed grape marc adsorbent exposed to cement plant flue gas with a desorption temperature of 120 °C.

Cycle number	q_e(mg/g)
1	40.44
2	36.31
3	36.07
4	32.03

cycle is presented in Table 11. However, more experimental data is needed for obtaining a correlation between the adsorbent deactivation and the number of adsorption/desorption cycles.

4. Conclusion

In this study, carbon-based adsorbents were synthetized from residues of cork stoppers, grape marc, and rice husk via pyrolysis and hydrothermal carbonization with and without lanthanum functionalization. The results show pyrolysis is the preferred method for synthesizing CO_2 adsorbents from these materials, as it leads to higher carrying capacities (up to 63 mg CO_2 /g adsorbent). When testing the multicyclic performance of the adsorbents at atmospheric pressure and using moderate temperatures for adsorption and desorption, no deactivation was detected within the 5 cycles tested, except for the grape marc-based adsorbent in the presence of flue gas. This means that in the case of cork- and rice husk-based adsorbents, the fresh adsorbent required is only for compensating the material loss in the separation units. Concerning the loss of activity of the grape marc–based adsorbent over consecutive cycles, it is explained by its slower kinetic performance, which may lead to incomplete desorption. It is expected that longer desorption times would reduce this deactivation. Regarding lanthanum functionalization, it was detected a positive effect for the CO_2 adsorption properties of grape marc-based adsorbent. The hypothesis is that the lanthanum functionalization reduces the microporosity of the sample, increasing the rate of CO_2 adsorption. No positive effect was present when submitting the remaining adsorbents to lanthanum functionalization. The use of cement plant flue gas led to slower adsorption rates and lower equilibrium carrying capacities of the adsorbents, as expected. Nevertheless, the experimental equilibrium carrying capacity was higher than the one estimated based on the CO_2 content and on the kinetic constants. Further investigation is needed to evaluate the selectivity and long-term stability of these materials and to compare the costs of this process to benchmark technologies, such as MEA absorption.

CRediT authorship contribution statement

Ana S. Amorim: Writing – original draft, Visualization, Software, Methodology, Investigation, Formal analysis, Conceptualization. **Rui M. Filipe:** Writing – review & editing, Supervision, Methodology, Conceptualization. **Cintia K. Rojas-Mayorga:** Writing – review & editing, Supervision, Methodology, Investigation. **Didilia I. Mendoza-Castillo:** Writing – review & editing, Methodology, Investigation. **Adrián Bonilla–Petriciolet:** Writing – review & editing, Supervision, Resources, Methodology, Conceptualization. **Henrique A. Matos:** Writing – review & editing, Supervision, Project administration, Methodology, Funding acquisition, Conceptualization.

Declaration of competing interest

The authors declare that they have no known competing financial interests or personal relationships that could have appeared to influence the work reported in this paper.

Acknowledgements

This work was supported by c^{5}Lab – Sustainable Construction Materials Association [CENTRO-04-3559-FSE-000096; LISBOA-05-3559-FSE-000008; C05-i02/2022], CERENA [FCT Project UID/04028/2025, https://doi.org/10.54499/UID/04028/2025] and the European Union's Horizon 2020 research and innovation program under the Marie Sklodowska-Curie grant agreement no. 778168.

Appendix A. Supplementary data

Supplementary data to this article can be found online at https://doi.org/10.1016/j.ces.2026.123637.

Data availability

Data will be made available on request.

References

Akdag, A.S., Durán, I., Gullu, G., Pevida, C., 2022. Performance of TSA and VSA post-combustion CO2 capture processes with a biomass waste-based adsorbent. J. Environ. Chem. Eng. 10. https://doi.org/10.1016/J.JECE.2022.108759.

Annual CO_2 emissions from cement 2023. https://ourworldindata.org/grapher/annual-co2-cement (accessed May 23, 2025).

Apolloni, F., Menegazzo, F., Bittencourt, C., Signoretto, M., 2025. Hazelnut shells and rice husks activated biochars for the adsorption of atrazine and terbuthylazine. next. Energy 7. https://doi.org/10.1016/J.NXENER.2025.100291.

Casal, M.D., Díez, N., Payá, S., Sevilla, M., 2023. Cork-derived carbon sheets for high-performance na-ion capacitors. ACS Appl. Energy Mater. 6, 8120–8131. https://doi.org/10.1021/ACSAEM.3C01212/ASSET/IMAGES/LARGE/AE3C01212_0008.JPEG.

CO_2 emissions - Our World in Data 2023. https://ourworldindata.org/co2-emissions (accessed May 23, 2025).

Cognigni, P., Leonelli, C., Berrettoni, M., 2025. A bibliographic study of biochar and hydrochar: differences and similarities. J. Anal. Appl. Pyrol. 187, 106985. https://doi.org/10.1016/J.JAAP.2025.106985.

da Rocha J de G, Santana Junior MB, Pier Macuvele DL, Riella HG, Ienczak JL, Padoin N, et al. Uncovering engineering and mechanistic insights in green synthesis of carbon dots from rice husks. Chemical Engineering Journal 2025;505:159364. https://doi.org/10.1016/J.CEJ.2025.159364.

Debastiani, R., Iochims dos Santos, C.E., Ferraz, D.J., 2021. Elemental characterization of sparkling wine and cork stoppers. Curr. Res. Food Sci. 4, 670–678. https://doi.org/10.1016/J.CRFS.2021.09.006.

Deiana, A., Gimenez, M., Rómoli, S., Sardella, M., Sapag, K., 2014. Batch and column studies for the removal of lead from aqueous solutions using activated carbons from viticultural industry wastes. Adsorpt. Sci. Technol. 32, 181–195. https://doi.org/10.1260/0263-6174.32.2-3.181.

del Pozo, C., Rego, F., Puy, N., Bartrolí, J., Fàbregas, E., Yang, Y., et al., 2022. The effect of reactor scale on biochars and pyrolysis liquids from slow pyrolysis of coffee silverskin, grape pomace and olive mill waste, in auger reactors. Waste Manag. 148, 106–116. https://doi.org/10.1016/J.WASMAN.2022.05.023.

Dhingra, G., Kumar, A., 2025. Carbon Capture and Sequestration: Cutting-Edge Technologies to Combat climate Change. Sustainable Energy Technol. Assess. 75, 104226. https://doi.org/10.1016/J.SETA.2025.104226.

Diaz E, Manzano FJ, Villamil J, Rodriguez JJ, Mohedano AF. Low-Cost Activated Grape Seed-Derived Hydrochar through Hydrothermal Carbonization and Chemical Activation for Sulfamethoxazole Adsorption. Applied Sciences 2019, Vol 9, Page 5127 2019;9:5127. https://doi.org/10.3390/APP9235127.

Domingos, D.G., Barcelos, K.M., Oliveira, K.S.G.C., Juchen, P.T., Ruotolo, L.A.M., Hassemer, M.E.N., 2024. Cork activated carbon as a new sustainable electrode for electrochemical desalination: customized surface chemistry for improved performance. Electrochim. Acta 507, 145120. https://doi.org/10.1016/J.ELECTACTA.2024.145120.

dos Santos, C.E.I., Debastiani, R., Przybylowicz, W., Manfroi, V., Amaral, L., Yoneama, M.L., et al., 2013. Study of the elemental composition of wine stoppers using PIXE. X-Ray Spectrom. 42, 158–164. https://doi.org/10.1002/XRS.2451.

Drage, T.C., Kozynchenko, O., Pevida, C., Plaza, M.G., Rubiera, F., Pis, J.J., et al., 2009. Developing activated carbon adsorbents for pre-combustion CO2 capture. Energy Procedia 1, 599–605. https://doi.org/10.1016/J.EGYPRO.2009.01.079.

Engel, J.B., Luchese, C.L., Tessaro, I.C., 2022. Characterization techniques comparison towards a better understanding of different cork-based stoppers types. J. Food Eng. 328, 111063. https://doi.org/10.1016/J.JFOODENG.2022.111063.

Frikha, K., Limousy, L., Arif, M.B., Thevenin, N., Ruidavets, L., Zbair, M., et al., 2021. Exhausted grape marc derived biochars: effect of pyrolysis temperature on the yield and quality of biochar for soil amendment. Sustainability 13. https://doi.org/10.3390/su132011187.

Gao, Y., Wang, X., Wang, J., Li, X., Cheng, J., Yang, H., et al., 2013. Effect of residence time on chemical and structural properties of hydrochar obtained by hydrothermal carbonization of water hyacinth. Energy 58, 376–383. https://doi.org/10.1016/J.ENERGY.2013.06.023.

García-Laynez, M.C., Herrera, M., Molina, S.I., Sanz de León, A., 2025. Chitin nanocrystals as bio-based adhesives for the development of sustainable cork composites. Carbohydr. Polym. Technol. Appl. 10, 100783. https://doi.org/10.1016/J.CARPTA.2025.100783.

Gong, J., Liu, R., Sun, Y., Xu, J., Liang, M., Sun, Y., et al., 2024. Preparation of high-performance nitrogen doped porous carbon from cork biomass by K2CO3 activation for adsorption of rhodamine B. Ind. Crop. Prod. 208, 117846. https://doi.org/10.1016/J.INDCROP.2023.117846.

Henrotin, A., Heymans, N., Duprez, M.E., Mouchaham, G., Serre, C., Wong, D., et al., 2024. Lab-scale pilot for CO2 capture vacuum pressure swing adsorption: MIL-160 (Al) vs zeolite 13X. Carbon Capture Sci. Technol. 12, 100224. https://doi.org/10.1016/J.CCST.2024.100224.

Ismail, I.S., Singh, G., Smith, P., Kim, S., Yang, J.H., Joseph, S., et al., 2020. Oxygen functionalized porous activated biocarbons with high surface area derived from grape marc for enhanced capture of CO2 at elevated-pressure. Carbon N Y 160, 113–124. https://doi.org/10.1016/J.CARBON.2020.01.008.

Ketabchi, M.R., Babamohammadi, S., Davies, W.G., Gorbounov, M., Masoudi, S.S., 2023. Latest advances and challenges in carbon capture using bio-based sorbents: A state-of-the-art review. Carbon Capture Science and Technology 6, 100087. https://doi.org/10.1016/j.ccst.2022.100087.

Krishnan, A., Nighojkar, A., Kandasubramanian, B., 2023. Emerging towards zero carbon footprint via carbon dioxide capturing and sequestration. Carbon Capture Sci. Technol. 9, 100137. https://doi.org/10.1016/J.CCST.2023.100137.

Kumar, P.R., Maharajan, T.M., Prabu, A.P., Santhana Kumar, K., Kumar, R., Maharajan, M., et al., 2019. Hydroxyl radical scavenging activity of La 2 O 3 nanoparticles. ~ 759 ~ the Pharma Innovation Journal 8, 759–763.

Li, Z., Feng, S., Yang, X., Lyu, H., Wei, S., Shen, B., 2025. A review of biomass porous carbon for carbon dioxide adsorption from flue gas: Physicochemical properties and performance. Fuel 387, 134318. https://doi.org/10.1016/J.FUEL.2025.134318.

Li, S., Yuan, X., Deng, S., Zhao, L., Lee, K.B., 2021. A review on biomass-derived CO2 adsorption capture: Adsorbent, adsorber, adsorption, and advice. Renew. Sustain. Energy Rev. 152, 111708. https://doi.org/10.1016/J.RSER.2021.111708.

Li, Y., Zhang, D., Li, W., Lan, Y., Li, Y., 2020. Efficient removal of As(III) from aqueous solution by S-doped copper-lanthanum bimetallic oxides: Simultaneous oxidation and adsorption. Chem. Eng. J. 384, 123274. https://doi.org/10.1016/J.CEJ.2019.123274.

Liu, J., Zhong, X., Chen, G., 2025. Designing guidelines of coal-based porous carbon for CO2 capture under flue gas conditions: A review. Chem. Eng. J. 511, 162029. https://doi.org/10.1016/J.CEJ.2025.162029.

Madadian, E., Rahimi, J., Mohebbi, M., Simakov, D.S.A., 2022. Grape pomace as an energy source for the food industry: a thermochemical and kinetic analysis. Food Bioprod. Process. 132, 177–187. https://doi.org/10.1016/J.FBP.2022.01.006.

Mansaray, K.G., Ghaly, A.E., 1998. Thermogravimetric analysis of rice husks in an air atmosphere. Energy Source. 20, 653–663. https://doi.org/10.1080/00908319808970084.

Manyà JJ, García-Morcate D, González B. Adsorption Performance of Physically Activated Biochars for Postcombustion CO2 Capture from Dry and Humid Flue Gas. Applied Sciences 2020, Vol 10, Page 376 2020;10:376. https://doi.org/10.3390/APP10010376.

Mendoza-Castillo DI, Reynel-Ávila HE, L. di B, Pastore C, Bonilla-Petriciolet A. Preparation of lanthanum functionalized adsorbents from a lignocellulosic biomass and their application in arsenic adsorption. HERAKLION, 2019. https://doi.org/10.5281/ZENODO.3834863.

Merodio-Morales, E.E., Mendoza-Castillo, D.I., Bonilla-Petriciolet, A., Reynel-Avila, H.E., Milella, A., di Bitonto, L., et al., 2022. A novel CO2 activation at room temperature to prepare an engineered lanthanum-based adsorbent for a sustainable arsenic removal from water. Chem. Eng. Res. Des. 185, 239–252. https://doi.org/10.1016/J.CHERD.2022.07.003.

Montero, I., Miranda, T., Sepúlveda, F.J., Arranz, I., Nogales, S., 2014. Analysis of Pelletizing of Granulometric Separation Powder from Cork Industries. Materials 7, 6686–6700. https://doi.org/10.3390/ma7096686.

Paz, L., Gentil, S., Fierro, V., Celzard, A., 2024. Assessing the performance of adsorbents for CO2/CH4 separation in pressure swing adsorption units: a review. J. Environ. Chem. Eng. 12, 114870. https://doi.org/10.1016/J.JECE.2024.114870.

Qi, R., Chen, Z., Wang, M., Wu, R., Jiang, E., 2019. Prediction method for torrefied rice husk based on gray-scale analysis. ACS Omega 4, 17837–17842. https://doi.org/10.1021/ACSOMEGA.9B02478/ASSET/IMAGES/LARGE/AO9B02478_0006.JPEG.

Quan, C., Zhou, Y., Wang, J., Wu, C., Gao, N., 2023. Biomass-based carbon materials for CO2 capture: a review. J. CO2 Util. 68. https://doi.org/10.1016/J.JCOU.2022.102373.

Quang, N.K., Hieu, N.N., Bao, V.V.Q., Phuoc, V.T., Ngoc, L.X.D., Doc, L.Q., et al., 2022. Hydrothermal synthesis of carbon nanodots from waste wine cork and their use in biocompatible fluorescence imaging. New Carbon Mater. 37, 595–602. https://doi.org/10.1016/S1872-5805(22)60608-5.

Querejeta, N., Gil, M.V., Rubiera, F., Pevida, C., Wawrzyńczak, D., Panowski, M., et al., 2024. Bio-engineering of carbon adsorbents to capture CO2 from industrial sources: the cement case. Sep. Purif. Technol. 330, 125407. https://doi.org/10.1016/J.SEPPUR.2023.125407.

Ren, T., Liu, L., Jing, Y., Dou, M., Wang, J., Chen, X., et al., 2025. Exploring enhanced CO2 separation from blast furnace gas: A multicolumn vacuum swing adsorption approach with process design and experimental assessment. Sep. Purif. Technol. 354, 129300. https://doi.org/10.1016/J.SEPPUR.2024.129300.

Rezvani, B., Hallajisani, A., Tavakoli, O., 2025. Super-effective biochar adsorbents from Co-pyrolysis of rice husk and sewage sludge: Adsorption performance, advanced regeneration, and economic analysis. Bioresour. Technol. Rep. 29, 102046. https://doi.org/10.1016/J.BITEB.2025.102046.

Shangguan, W., Chen, Z., Zhao, J., Song, X., 2018. Thermogravimetric analysis of cork and cork components from Quercus variabilis. Wood Sci. Technol. 52, 181–192. https://doi.org/10.1007/S00226-017-0959-9.

Si, H., Hong, Q., Chen, X.H., Jiang, L., 2025. Pressure swing adsorption for oxygen production: Adsorbents, reactors, processes and perspective. Chem. Eng. J. 509, 161273. https://doi.org/10.1016/J.CEJ.2025.161273.

Sifat, N.S., Haseli, Y., 2019. A critical review of CO2 capture technologies and prospects for clean power generation. Energies (basel) 12. https://doi.org/10.3390/EN12214143.

Singh, G., Lakhi, K.S., Sil, S., Bhosale, S.V., Kim, I.Y., Albahily, K., et al., 2019. Biomass derived porous carbon for CO2 capture. Carbon N Y 148, 164–186. https://doi.org/10.1016/J.CARBON.2019.03.050.

Titone, V., Rapisarda, M., Pulvirenti, L., Napoli, E., Impallomeni, G., Botta, L., et al., 2025. Sustainable biocomposites based on Mater-Bi and grape pomace for a circular economy: Performance evaluation and degradation in soil. Polym. Degrad. Stab. 231, 111091. https://doi.org/10.1016/J.POLYMDEGRADSTAB.2024.111091.

Wang, Q., Chu, D., Luo, C., Lai, Z., Shang, S., Rahimi, S., et al., 2022. Transformation mechanism from cork into honeycomb–like biochar with rich hierarchical pore structure during slow pyrolysis. Ind. Crop. Prod. 181, 114827. https://doi.org/10.1016/J.INDCROP.2022.114827.

Wang, S., Zhang, S., Du, X., Shen, Y., Ma, Z., 2019. Effect of lanthanum doping on the microstructure, thermal stability, and CO 2 adsorption property of ZIF-8. Adv. Mater. Sci. Eng. https://doi.org/10.1155/2019/9734984.

Zhang, P., Wang, L., 2025. Temperature swing adsorption cycle with recovered gas injection. Chem. Eng. Res. Des. 217, 121–127. https://doi.org/10.1016/J.CHERD.2025.03.025.

Zhao, R., Liu, L., Zhao, L., Deng, S., Li, S., Zhang, Y., 2019. A comprehensive performance evaluation of temperature swing adsorption for post-combustion carbon dioxide capture. Renew. Sustain. Energy Rev. 114, 109285. https://doi.org/10.1016/J.RSER.2019.109285.

Zhu, S., Zhao, B., Zhang, H., Su, Y., 2023. Biomass-based adsorbents for post-combustion CO2 capture: Preparation, performances, modeling, and assessment. J. Environ. Manage. 328, 117020. https://doi.org/10.1016/J.JENVMAN.2022.117020.

Zuazua Ruiz, A., Martín Martín, J.M., Prados-Castillo, J.F., 2023. The European Union facing climate change: a window of opportunity for technological development and entrepreneurship. Sustainable Technol. Entrepreneurship 2, 100035. https://doi.org/10.1016/J.STAE.2022.100035.